



HAL
open science

Solar Soft X-ray Irradiance Variability, I: Segmentation of Hinode/XRT Full-Disk Images and Comparison with GOES (1 – 8 Å) X-Ray Flux

H. N. Adithya, Rangaiah Kariyappa, Imada Shinsuke, Kusano Kanya, Joe Zender, Luc Damé, Giono Gabriel, Edward Deluca, Mark Weber

► **To cite this version:**

H. N. Adithya, Rangaiah Kariyappa, Imada Shinsuke, Kusano Kanya, Joe Zender, et al.. Solar Soft X-ray Irradiance Variability, I: Segmentation of Hinode/XRT Full-Disk Images and Comparison with GOES (1 – 8 Å) X-Ray Flux. *Solar Physics*, 2021, 296 (4), pp.art. 71. 10.1007/s11207-021-01785-6 . insu-03203005

HAL Id: insu-03203005

<https://insu.hal.science/insu-03203005>

Submitted on 28 Nov 2022

HAL is a multi-disciplinary open access archive for the deposit and dissemination of scientific research documents, whether they are published or not. The documents may come from teaching and research institutions in France or abroad, or from public or private research centers.

L'archive ouverte pluridisciplinaire **HAL**, est destinée au dépôt et à la diffusion de documents scientifiques de niveau recherche, publiés ou non, émanant des établissements d'enseignement et de recherche français ou étrangers, des laboratoires publics ou privés.



Solar Soft X-ray Irradiance Variability, I: Segmentation of Hinode/XRT Full-Disk Images and Comparison with GOES (1–8 Å) X-Ray Flux

H.N. Adithya^{1,2} · Rangaiah Kariyappa^{3,2}  · Imada Shinsuke² · Kusano Kanya² · Joe Zender⁴ · Luc Damé⁵ · Giono Gabriel⁶ · Edward DeLuca⁷ · Mark Weber⁷

Received: 5 August 2020 / Accepted: 12 February 2021 / Published online: 20 April 2021
© The Author(s), under exclusive licence to Springer Nature B.V. 2021

Abstract It is of great interest and importance to study the variabilities of solar EUV, UV and X-ray irradiance in heliophysics, in Earth's climate, and space weather applications. A careful study is required to identify, track, monitor and segment the different coronal features such as active regions (ARs), coronal holes (CHs), the background regions (BGs) and the X-ray bright points (XBPs) from spatially resolved full-disk images of the Sun. Variability of solar soft X-ray irradiance is studied for a period of 13 years (February 2007–March 2020, covers Solar Cycle 24), using the X-Ray Telescope on board the Hinode (Hinode/XRT) and GOES (1–8 Å). The full-disk X-ray images observed in Al₁ mesh filter from XRT are used, *for the first time*, to understand the solar X-ray irradiance variability measured, Sun as a star, by GOES instrument. An algorithm in Python has been developed and applied to identify and segment coronal X-ray features (ARs, CHs, BGs, and XBPs) from the full-disk soft X-ray observations of Hinode/XRT. The segmentation process has been carried out automatically based on the intensity level, morphology and sizes of the X-ray features. The total intensity, area, and contribution of ARs/CHs/BGs/XBPs features were estimated and compared with the full-disk integrated intensity (FDI) and GOES (1–8 Å) X-ray irradiance measurements. The XBPs have been identified and counted automatically over the full disk to investigate their relation to solar magnetic cycle. The total

✉ R. Kariyappa
rkari@iiap.res.in

H.N. Adithya
adithyabhattsringeri@gmail.com

- 1 Young Innovators Educational Services Pvt. Ltd (YIESPL), Bangalore 560040, India
- 2 Institute for Space-Earth Environmental Research (ISEE), Nagoya University, Nagoya, Japan
- 3 Indian Institute of Astrophysics, Bangalore 560034, India
- 4 European Space Research and Technology Center (ESTEC), 2200 AG Noordwijk, The Netherlands
- 5 LATMOS (Laboratoire Atmosphères, Milieux, Observations Spatiales), 11 boulevard d'Alembert, 78280 Guyancourt, France
- 6 Department of Space and Plasma Physics, School of Electrical Engineering, Royal Institute of Technology KTH, 10044 Stockholm, Sweden
- 7 Harvard-Smithsonian Center for Astrophysics, 60 Garden Street, Cambridge, MA, USA

intensity of ARs/CHs/BGs/XBPs/FD regions are compared with the GOES (1–8 Å) X-ray irradiance variations. We present the results obtained from Hinode/XRT full-disk images (in Al_{mesh} filter) and compare the resulting integrated full-disk intensity (FDI) with GOES X-ray irradiance. The X-ray intensity measured over ARs/CHs/BGs/XBPs/FD is well correlated with GOES X-ray flux. The contributions of the segmented X-ray features to FDI and X-ray irradiance variations are determined. It is found that the background and active regions have a greater impact on the X-ray irradiance fluctuations. The mean contribution estimated for the whole observed period of the background regions (BGs) will be around $65 \pm 10.97\%$, whereas the ARs, XBPs and CHs are $30 \pm 11.82\%$, $4 \pm 1.18\%$ and $1 \pm 0.52\%$, respectively, to total solar X-ray flux. We observed that the area and contribution of ARs and CHs varies with the phase of the solar cycle, whereas the BGs and XBPs show an anti-correlation. We find that the area of the coronal features is highly variable suggesting that their area has to be taken into account in irradiance models, in addition to their intensity variations. The time series results of XBPs suggest for an existence of anti-correlation between the number of XBPs and the sunspot numbers. It is also important to consider both the number variation and the contribution of XBPs in the reconstruction of total solar X-ray irradiance variability.

Keywords Sun: X-ray radiation · Sun: corona · Sun: coronal features · Sun: X-ray bright points

1. Introduction

The radiant energy from the Sun is the primary source of energy to the Earth. This radiant energy is measured and reported as the solar irradiance. It is known that the Total Solar Irradiance (TSI) is a measure of total radiation over the entire electromagnetic spectrum and that when measured as a function of wavelength, it is called spectral irradiance. Since the radiative output of the Sun is one of the main driving forces of the terrestrial atmosphere and climate system, the study of solar energy has become of great interest and importance. Although the solar energy flux integrated over the entire spectrum is considered to be one of the major natural forces of the Earth's climate system, studying the extreme ultraviolet (EUV), ultraviolet (UV) and X-ray irradiance variability is particularly important in solar and terrestrial physics. The solar EUV, UV and X-ray fluxes play in particular a major role in the heating of the Earth's atmosphere and Solar-Terrestrial relationships. Thus it is an important issue to understand their variability and its applications in Earth's climate and space weather.

The total solar irradiance (TSI) has been monitored from several satellites for more than three decades. It has been observed and reported that the solar energy flux changes over a solar magnetic cycle. The long-term irradiance variations are due to the changing emission of bright magnetic elements e.g. (Foukal and Lean, 1988; Kariyappa and Pap, 1996; Worden, White, and Woods, 1998; Kariyappa, 2000, 2008b; Veselovsky et al., 2001; Kumara et al., 2012, 2014; Zender et al., 2017), and the short-term irradiance variations are directly related to active regions as they evolve, fragment, and move across the solar disk (Lean, 1987; Giono et al., 2021; van der Zwaard et al., 2021). The reason for the difference between the observed and modeled solar irradiance variability and the underlying physical mechanisms of solar irradiance variability are not yet fully understood. Recently some studies have been done to estimate the contribution of various coronal features to EUV and UV irradiance using spatially resolved observations (Kumara et al., 2014; Zender et al., 2017). These authors

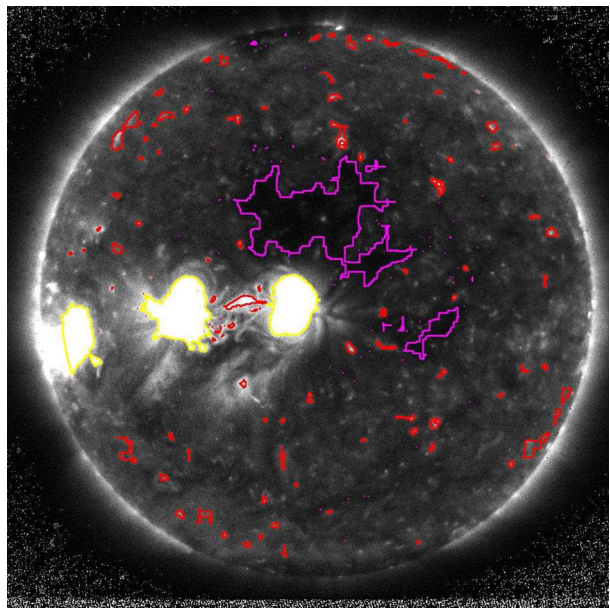
used full-disk images from PROBA2/SWAP and SDO/AIA and segmented different coronal features to understand the EUV and UV irradiance measured by the PROBA2/LYRA instrument. In addition they investigated and discussed in detail the role of magnetic field on EUV and UV irradiance variability by comparing SWAP and AIA images with SDO/HMI magnetograms. Since all features are quite dynamic in nature, and their morphological structure and magnetic configuration will continuously change, the segmentation of coronal features from the images is a difficult task.

The history of solar soft X-ray radiation (SXR) observations can be traced back to the 1960s. The measurements from sounding rockets have led to several satellite-based experiments, including SOLRAD (Dere, Horan, and Kreplin, 1974), Orbiting Solar Observatory (Hall and Hinteregger, 1970), SkyLab (1973–1979) (Vaiana et al., 1976), and Solar Maximum Mission (Acton et al., 1980). The Soft X-ray Telescope (SXT) on Yohkoh observed the full-disk of the Sun in the wavelength range from 0.2 to 3 nm from 1991 to 2001 (Ogawara et al., 1992). Acton, Weston, and Bruner (1999) have determined the solar X-ray irradiance using an isothermal spectral model and differential emission measure (DEM). The Soft X-ray Photometer on the Student Nitric Oxide Explorer (SNOE) had several broadband channels taking daily measurements of solar X-ray irradiance with three band-passes of 2–7 nm, 6–19 nm, and 17–20 nm (Bailey et al., 2000, 2006). The Geostationary Operational Environmental Satellite (GOES) of the National Oceanic and Atmospheric Administration (NOAA) has a series of satellites carrying X-Ray Sensor (XRS), measuring X-ray flux at 0.5–4 Å (XRS-A) and 1–8 Å (XRS-B) (Viereck and Machol, 2017). An attempt has been made to estimate a soft X-ray (SXR) background flux by subtracting out the contribution of solar flares using the soft X-ray observations from GOES (1–8 Å). It is observed that the post-flare emission from a bright active regions appears to play a dominant role in the SXR background flux variations, whereas the quiet Sun contributions to SXR background flux are significant during solar minimum. The comparison studies of SXR irradiance values with full-disk integrated images from Yohkoh suggest that the presence of coronal holes can reduce the SXR irradiance level only in the rare case of absence of active regions (Aschwanden, 1994).

GOES is measuring solar X-ray flux daily and its variations need to be understood from spatially resolved full-disk soft X-ray images. In particular, the segmentation of different coronal features from the X-ray images has not been done. It is important to know: (i) how the different coronal features contribute to the total solar X-ray irradiance variability, particularly the quiet Sun component (both background—BGs—and XBPs), (ii) how do they help in understanding the Sun-as-a-star total solar flux measured, (iii) how they are related to underlying photospheric magnetic features and (iv) the role of magnetic field on the X-ray irradiance variability.

In this paper, we made an attempt to address some of the problems mentioned above using, *for the first time*, the observations from the Hinode/XRT and GOES instruments. For this purpose, we use an algorithm developed by us in Python, which segments active regions (ARs), coronal holes (CHs), background regions (BGs), and X-ray Bright Points (XBPs) more accurately. The whole segmentation procedure has been carried out with more precise, accurate, fast, stable in both time and space, allowing for a detailed analysis of spatially resolved full-disk images and solar X-ray flux. The details of the observations, analysis, results of intensity, area, and contribution of ARs, CHs, BGs, XBPs, full-disk intensity (FDI), and GOES (1–8 Å) flux are presented and discussed.

Figure 1 A sample of the segmented image observed with the A1_mesh filter, showing all the features: ARs (yellow), CHs (violet), BGs (rest) and XBPs (red) obtained with Hinode/XRT on March 27, 2008.



2. Observations and Analysis

We used full-disk daily images taken by the X-Ray Telescope on board the Hinode mission (Hinode/XRT). The details on the design, calibration, and measured performance of the XRT instrument up to the focal plane and the CCD camera and data handling are discussed in Kosugi et al. (2007) and Golub et al. (2007). The level-2 data from February 14, 2007 to March 31, 2020 was downloaded from http://solar.physics.montana.edu/HINODE/XRT/SCIA/synopi_images/syncmp_FITS. The xrt_prep procedure has been already applied, which subtracts a dark frame, carries out the vignetting correction, the removal of high-frequency noise, and the normalization by exposure time. In addition, the quality of the archived full-disk images has been further improved with the following three methods: (i) Images are composites of long+short exposure images to provide extended dynamic ranges and to eliminate saturations, (ii) small contamination of spots on the CCD have been corrected in the images by replacing affected pixels with the averaged intensity of the surrounding area, and (iii) the pointing information has been updated with a recently developed database that co-aligns XRT with other solar instruments (Takeda, Yoshimura, and Saar, 2016). The XRT data-set used in this analysis contains composite images. It is difficult for XRT to take a single image that sees both faint and bright features, hence the composite synoptic data sets include both long and short exposure images to observe both faint and bright features. Therefore, the composite image can represent a greater dynamic range than the instrument itself is capable of producing in a single image and the composite images were suitable to use for this analysis of all the features. Images of 2007 have 2048×2048 pixels and after 2008 all images are 1024×1024 pixels in size. Out of XRT's eight diagnostic filters, we selected for a detailed analysis the images that used the A1-mesh filter, since for that set we find there are continuous observations, and because the amount of stray light is negligible throughout the studied period. An example of a segmented image obtained on March 27, 2008 with this filter is presented in Figure 1. Bad images and off centered images are manually removed for the analysis. The X-ray irradiance at Earth was observed from

X-ray Sensor (XRS) onboard Geostationary Operational Environmental Satellites (GOES), which observe the Sun as a star, it can provide solar X-ray fluxes for the wavelength bands of 1–8 Å (long channel) and 0.5–4 Å (short channel). We choose 1–8 Å which is closer to the XRT band. Currently there are four satellites operationally available. Since a good and continuous data set was not available for 2007–2020 from one mission, we collected 1-minute averaged data from GOES 10, GOES 11, GOES 12, GOES 14 and GOES 15. For a comparison study with sunspot numbers (SSN), we have downloaded the daily sunspot numbers from the link: <http://www.sidc.be/silso/datafiles>.

We developed an algorithm in Python to extract all the features (ARs, CHs, BGs, and XBPs) from the full-disk X-ray images of the Sun. Coronal features are differentiated based on their brightness/intensity level, size/area and morphological structures. In order to identify, segment and extract the features we choose the threshold methods. Coronal holes (CHs) are extracted by intensity threshold, active region (ARs) and X-ray bright points (XBPs) are extracted by both intensity and area/size threshold method.

In order to determine the average threshold values (for both intensity and size/area) for all the features, we have selected a large number of full-disk images distributed over the entire period (2007–2020) representing the different phases of the solar activity showing both active and quiet Sun. It means that we have determined the average threshold values using a large number of images when the Sun was both active and in quiet phase.

The following steps have been followed for extraction of on-disk features for the available filter:

- i) Using the FITS header, center of images is found and 0.96 of solar radii disk is extracted to avoid edge/limb brightening;
- ii) Active regions (ARs):
 - mean and median of the solar disk are calculated;
 - $2.5 \times$ mean value set as lower limit intensity threshold;
 - for threshold image morphological closing operation is done with 5×5 kernel;
 - all closed contours having area more than 1000 pixels are considered as active regions.
- iii) Coronal holes (CHs):
 - $0.3 \times$ median value set as upper limit intensity threshold;
 - for thresholds image contours are drawn after morphological closing operation;
 - morphological closing is done with a 15×15 kernel to remove noisy grains and increase the connectivity;
 - all contours are considered as CHs.
- iv) X-ray bright points (XBPs):
 - all detected ARs are masked over the solar disk (ARs are masked to avoid intense ARs' effect on XBPs detection);
 - once again mean value of AR-masked disk is calculated;
 - $1.7 \times$ mean value set as lower limit intensity threshold;
 - for threshold image morphological closing operation is done with 5×5 kernel to remove small noisy grains;
 - contours are drawn after morphological closing operation is done;
 - contours having area greater than 10 pixels and less than 1000 pixels are considered as XBPs.
- v) Background (BGs):
 - after removing all XBPs, ARs and CHs, the remaining solar disk area is considered as background regions.

We have calculated the total intensity of each feature (expressed in DN/sec or energy/area/time, – where DN is data units and represents the digitized measure of the amount of energy accumulated in a CCD pixel during an image exposure, so image exposure durations have been normalized out, and the units are directly comparable to GOES' W/m^2), the total area (total number of pixels) of each feature, and their contribution (%) to full-disk intensity (FDI). These values have been compared with total X-ray flux measurements from GOES. We estimated the standard deviation for the variations of intensity contributions of all the features.

3. Results and Discussion

Using our algorithm we segmented coronal X-ray features automatically from full-disk Hinode/XRT images observed in Al_mesh filter (Figure 1) for the period from February 14, 2007 to March 31, 2020, which covers Solar Cycle 24. We derived the corresponding total intensity, area (total number of pixels) and contribution of ARs/CHs/BGs/XBPs. We have compared the total intensity and area of ARs/CHs/BGs/XBPs to full-disk total X-ray intensity (FDI) and derived their contribution to FDI and GOES ($1-8 \text{ \AA}$) X-ray flux for each day for the whole period. We observed from the time series plots of ARs/CHs/BGs/XBPs/FDI taken with Al_mesh (Figure 2) in comparison with GOES and sunspot numbers that the intensity of all the features is well correlated with FDI, GOES total X-ray flux and sunspot numbers. This indicates that the long-term variability of segmented features and full-disk intensity shows a correlation with GOES ($1-8 \text{ \AA}$) solar X-ray flux and the sunspot numbers, this implies that the changes are in phase with the solar cycle. As observed from the time series plots, ARs and BG are well correlated to the total soft X-ray irradiance measured by GOES ($1-8 \text{ \AA}$), and the intensity of XBPs and CHs seem to be moderately correlated to FDI and GOES X-ray flux. This suggests that BGs and ARs have greater impact, influence and contribution to X-ray irradiance fluctuations whereas the XBPs and CHs appear to have a smaller contribution to FDI and GOES X-ray flux variations. The important results of these are discussed in detail in the following sections.

3.1. Integrated Intensity and Area Variations of All the Features in Comparison with Full-Disk Intensity (FDI) and GOES ($1-8 \text{ \AA}$) Flux

The time series of integrated intensity of each of the coronal features and full-disk intensity for the Hinode/XRT X-ray images observed with the Al_mesh filter, GOES ($1-8 \text{ \AA}$) X-ray flux and sunspot numbers (SSN) are shown in Figure 2. The intensity of all the features vary with the phase of the solar cycle. It is also clear from Figure 2 that on an average over the solar cycle the integrated intensity of BGs is larger than the integrated intensity of ARs, CHs, and XBPs, but the contribution of ARs will become more dominant around solar maximum. Note that the BG intensity values will be slightly contaminated by the fuzzy regions (brighter than BG and less brighter than ARs, as seen in Figure 1) present around the ARs while segmenting the features. However, this does not change the results and conclusions. We also noticed that there is good correlation between the intensity of all the features in comparison with GOES X-ray flux and sunspot numbers indicating that they vary with solar activity.

Along with integrated intensity, we have computed the total area (total number of pixels) of ARs, CHs, BGs, and XBPs for the whole period. We have plotted the area of all the features in Figure 3 for the whole observed period and these are compared with the integrated

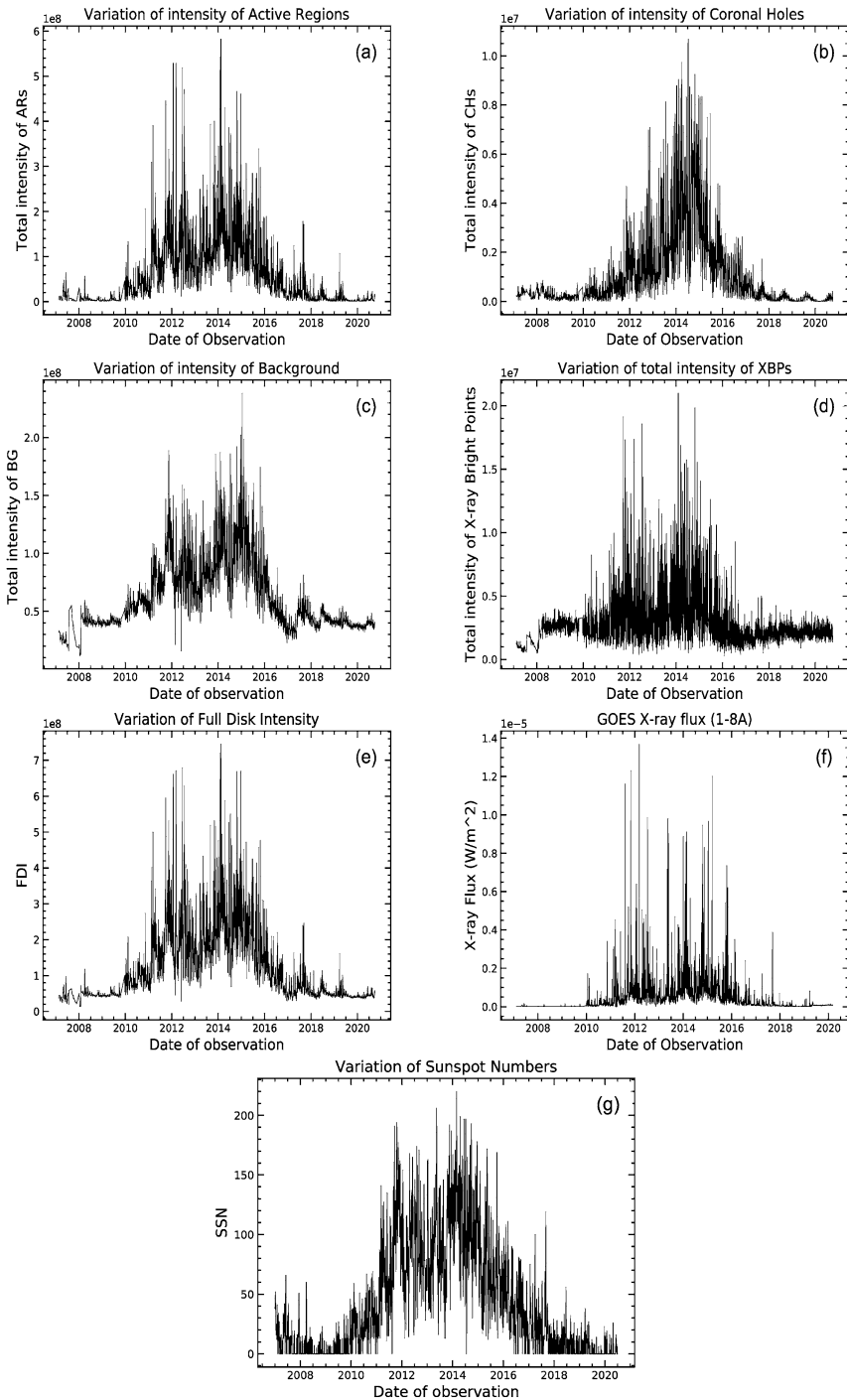


Figure 2 Total intensity of solar X-ray features: (a) ARs, (b) CHs, (c) BGs, (d) XBPs, (e) full-disk intensity (FDI) (observed by Hinode/XRT with the Al_{mesh} filter), (f) GOES (1–8 Å) X-ray flux, and (g) sunspot numbers (SSN) for a period starting from February 14, 2007 to March 31, 2020.

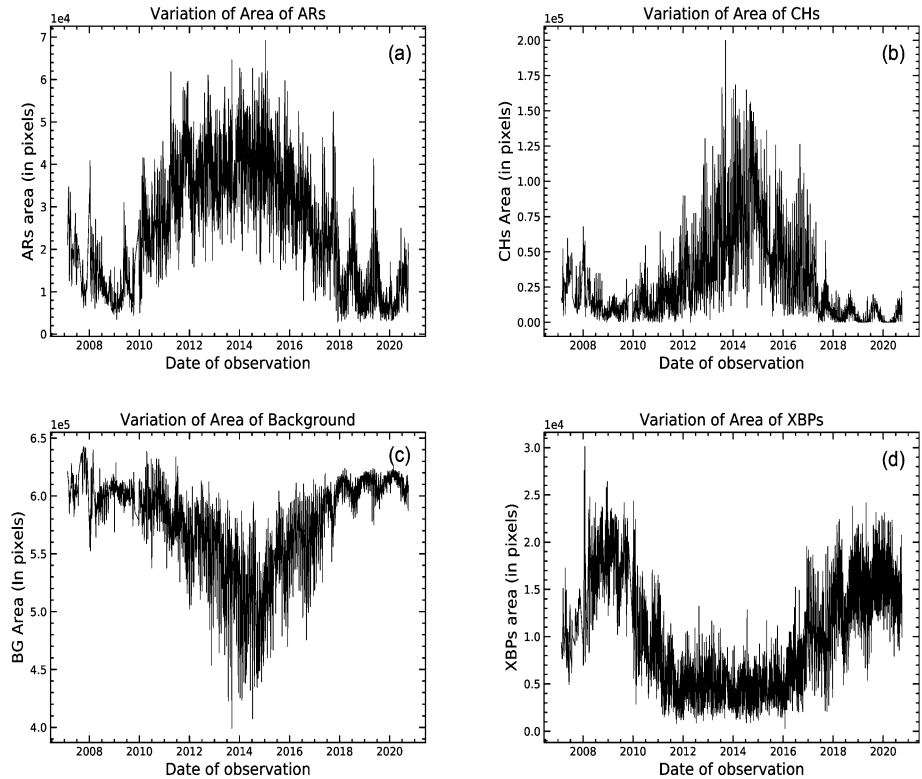


Figure 3 Total area (total number of pixels) variation of solar X-ray features: (a) ARs, (b) CHs, (c) BGs, and (d) XBPs (observed by Hinode/XRT with the Al_{mesh} filter) for a period starting from February 14, 2007 to March 31, 2020.

intensity of segmented features, FDI, GOES ($1 - 8 \text{ \AA}$), and SSN presented in Figure 2. From the times series shown in Figures 2 and 3, we noticed that the integrated intensity values and areas of all the features exhibit the expected 27 day modulation due to the solar rotation, similar to sunspots at the photospheric level. The features' area variation (shown in Figure 3) show that the area of ARs and CHs vary with the solar activity, whereas the BGs and XBPs are anti-correlated with the phase of the solar cycle. We estimated the mean areas of all the features for the whole observed period. Most importantly, from Figure 3 and the mean areas, we can clearly notice that the BGs cover ($5.82e + 5$ pixels) a very large portion of the Sun's surface, whereas ARs cover ($2.29e + 4$ pixels) slightly smaller area compared to CHs ($2.4e + 4$ pixels) and larger than XBPs ($1.07e + 4$ pixels) in general. We observed that the filling factors of ARs/CHs/BGs/XBPs evolve throughout the solar cycle and also find from Figure 3 that the area of the features is highly variable, similar to the integrated intensity variations seen in Figure 2. This means that the total intensity of each segmented feature is affected by the intensities of the feature itself and also by the changes of its area/size. The observed intensity variation is due to the change of feature's intensity and also due to the expansion/shrinkage of its area as it evolves. This suggests that the intensity and area of the coronal features have to be taken into account in the models to explain the irradiance variations.

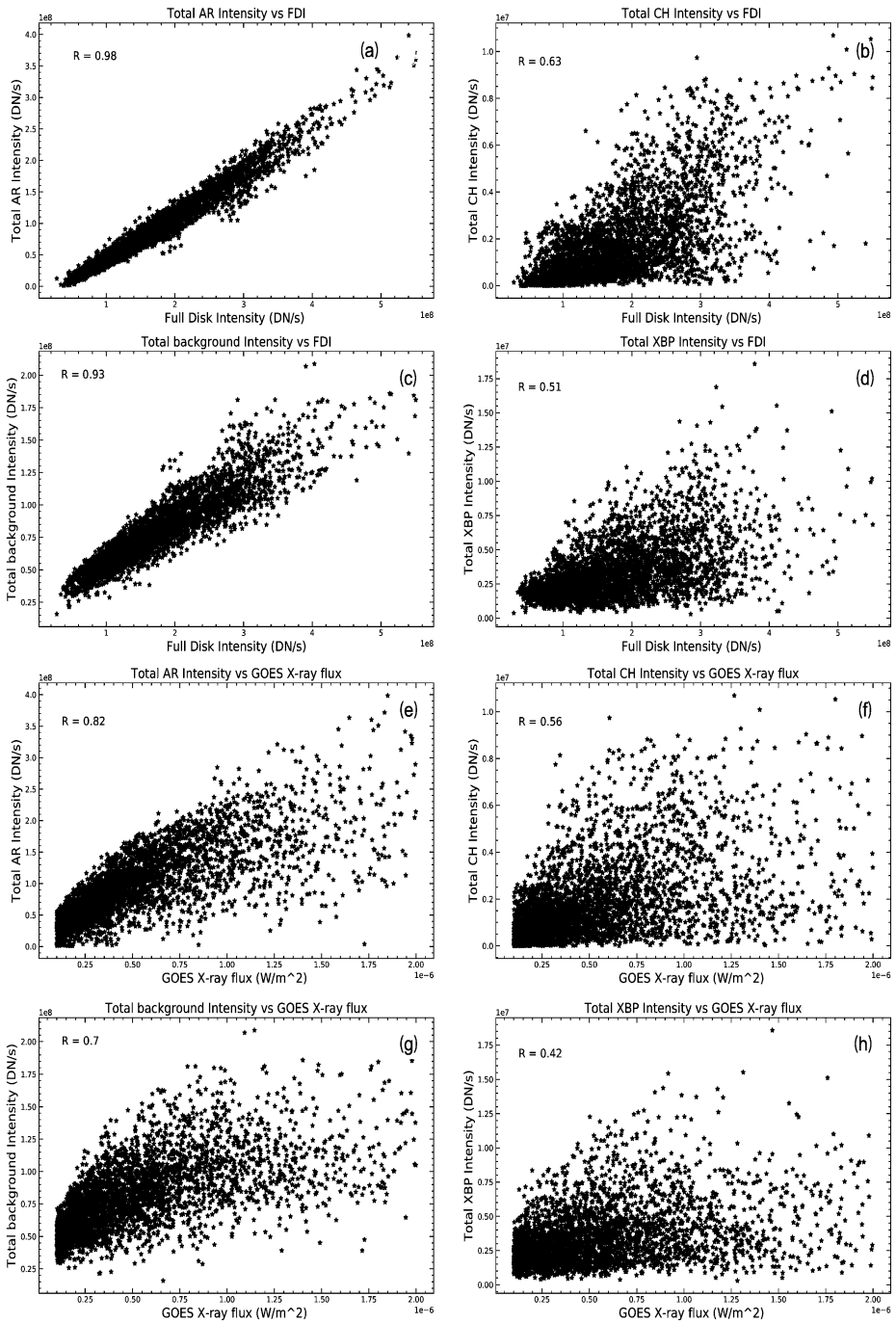


Figure 4 Using images taken with the Al_{mesh} filter, total intensity of all the features versus FDI and GOES flux: (a) ARs versus FDI, (b) CHs versus FDI, (c) BGs versus FDI, (d) XBPs versus FDI and (e) ARs versus GOES, (f) CHs versus GOES, (g) BGs versus GOES, (h) XBPs versus GOES and (i) FDI versus GOES. The correlation coefficient values (R) are marked on the top left corner of each plot.

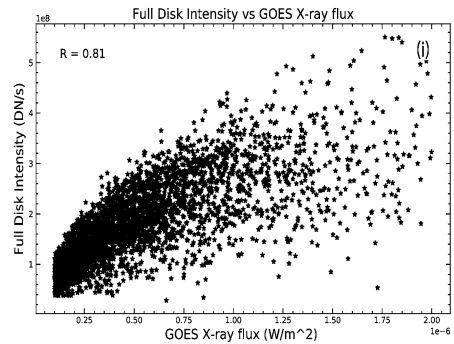
Figure 4 (Continued)

Table 1 Spearman rank correlation coefficients between GOES (1–8 Å) and full-disk intensity (FDI) with coronal features (ARs, BGs, CHs and XBPs) as observed with Hinode/XRT.

Correlation coefficients (R)	
Al_mesh filter (Figure 4)	
FDI vs GOES	0.81
CH vs GOES	0.56
XBPs vs GOES	0.42
AR vs GOES	0.82
BG vs GOES	0.70
CH vs FDI	0.63
XBPs vs FDI	0.51
AR vs FDI	0.98
BG vs FDI	0.93

In Figure 4, we have plotted for the Al_mesh filter the integrated intensity of all the features (ARs, CHs, BGs and XBPs) versus the full-disk intensity (FDI), GOES X-ray flux and sunspot numbers for a period of 13 years (February 2007–March 2020, covering Solar Cycle 24). We have determined the Spearman rank correlation coefficients of the segmented features with FDI and GOES solar X-ray irradiance values and their correlation coefficients (R) are presented in Table 1. As seen from the scatter plots (Figure 4) and the results of the correlation coefficients (in Table 1) for the Al_mesh filter, the ARs and BGs are well correlated to the total integrated intensity of the full-disk (XRT) and GOES X-ray irradiance measured in 1–8 Å. The mean correlation coefficient (R) values for ARs versus FDI and ARs versus GOES are 0.98 and 0.82, respectively. Similarly, the mean R values for BGs versus FDI and ARs versus GOES are 0.93 and 0.82, respectively. This suggests variations of ARs and BGs are of the same order of magnitude as the X-ray flux variations (although the physical units are different, the intensity is expressed in DN/s whereas the irradiance in calibrated units of W/m²). Therefore BGs and ARs have a greater impact and influence on the X-ray irradiance fluctuations. The XBPs and CHs show a correlation higher than R = 0.50 (average value of R with Al_mesh from Table 1) with FDI and GOES values, indicating XBPs and CHs will moderately contribute to the total X-ray irradiance fluctuations in addition to ARs and BGs. Since the XBPs and CHs are relatively low intensity features compared to the others, the results of XBPs and CHs are very sensitive to the thresholds used and hence we have tuned the algorithm's parameters precisely to obtain more accurate results. We noticed from Figure 4 and Table 1 that FDI measured from the spatially resolved images of the whole Sun is well correlated (R = 0.81) with GOES (1–8 Å) total X-ray flux measured Sun as

a star. However, we are aware that (i) there is no perfect overlap in the responses of XRT and GOES, and (ii) our analysis leaves out the solar limb and off-limb contributions to the variability. These points suggest that further work might be able to improve the correlation between XRT-observed features and the GOES total solar X-ray flux variability. We can conclude that the spatially resolved images are important asset to use to understand the integrated intensity variability of the Sun when we observe the Sun as a star (true also in the case of solar type stars, if they have stellar X-ray irradiance measurements, where we can use Sun as a calibrator).

3.2. Number Variation of XBPs with the Solar Magnetic Activity Cycle

Using our algorithm we have separated out the XBPs component from the quiet Sun areas, since quiet Sun is the combination of both background regions (BGs) and XBPs. In the case of EUV and UV image segmentation in our previous studies (Kumara et al., 2014; Zender et al., 2017) we did not separated out the bright points from the quiet Sun component, hence we had to deal with variations of the whole quiet Sun regions. In the present study, we have identified, (separated out background regions and XBPs), and extracted automatically the total number of XBPs based on their intensity levels, morphological structures and sizes (compared to other large scale features like ARs and masking them) over the full-disk images observed in *AI_mesh*), all this on a daily basis for the period of 13 years (February 2007–March 2020, which covers Solar Cycle 24).

In Figure 5(a), we have plotted the total number of XBPs extracted from *AI_mesh* filter as a function of time. In addition for a comparison study we have plotted in Figure 5(b), (c) and (d) the variation of FDI (for *AI_mesh* filter), GOES X-ray flux and sunspot numbers, respectively. We observed from these plots that the number of XBPs are inversely proportional to FDI, GOES X-ray flux and sunspot numbers. For more clarity we have also plotted in Figure 5(e) the number of XBPs observed in *AI_mesh* versus sunspot numbers (SSN) and it clearly indicates that there is an anti-correlation, with a mean correlation coefficient, $R = -0.86$, between the variation of XBPs numbers and the solar activity. Our investigations confirms the previous results of anti-correlation of number of XBPs with the solar cycle as derived in the quiet-Sun region from Yohkoh/SXT soft X-ray images (Hara and Nakakubo-Morimoto, 2004, 2003) and also with our recent results of variation of coronal bright points derived from the analysis of EUV and UV images (SDO/AIA and PROBA2/SWAP) by van der Zwaard et al. (2021). Several bright point detection algorithms implemented in long-term statistical analysis have been described, using Yohkoh/SXT (Nakakubo and Hara, 2000; Sattarov et al., 2002; Hara and Nakakubo-Morimoto, 2003, 2004), SOHO/EIT (McIntosh and Gurman, 2005; de Wit, 2006; McIntosh, 2007), or SDO/AIA (Alipour and Safari, 2015; Shahamatnia et al., 2016; Arish et al., 2016; Dorotovic et al., 2018) data as input. To counterweight the different intensity changes in EUV images both over the latitudinal range as well as the solar cycle changes, it has been discussed the need to apply an intensity background threshold to their BP detection algorithm (McIntosh and Gurman, 2005; McIntosh, 2007).

From an image analysis of a large sample of Kodaikanal Ca II K spectroheliograms, the intensity and area of the magnetic network elements at the center of the solar disk over two solar cycles have been estimated. From this study, it has been shown that the magnetic network elements occupy a larger area during solar minimum compared to solar maximum period (Kariyappa and Sivaraman, 1994), indicating that the network area is anti-correlated with the solar activity. Meanwhile it has been reported (Sivaraman, 1984) that the total number of bright points that are located in the interior of the network elements show a larger

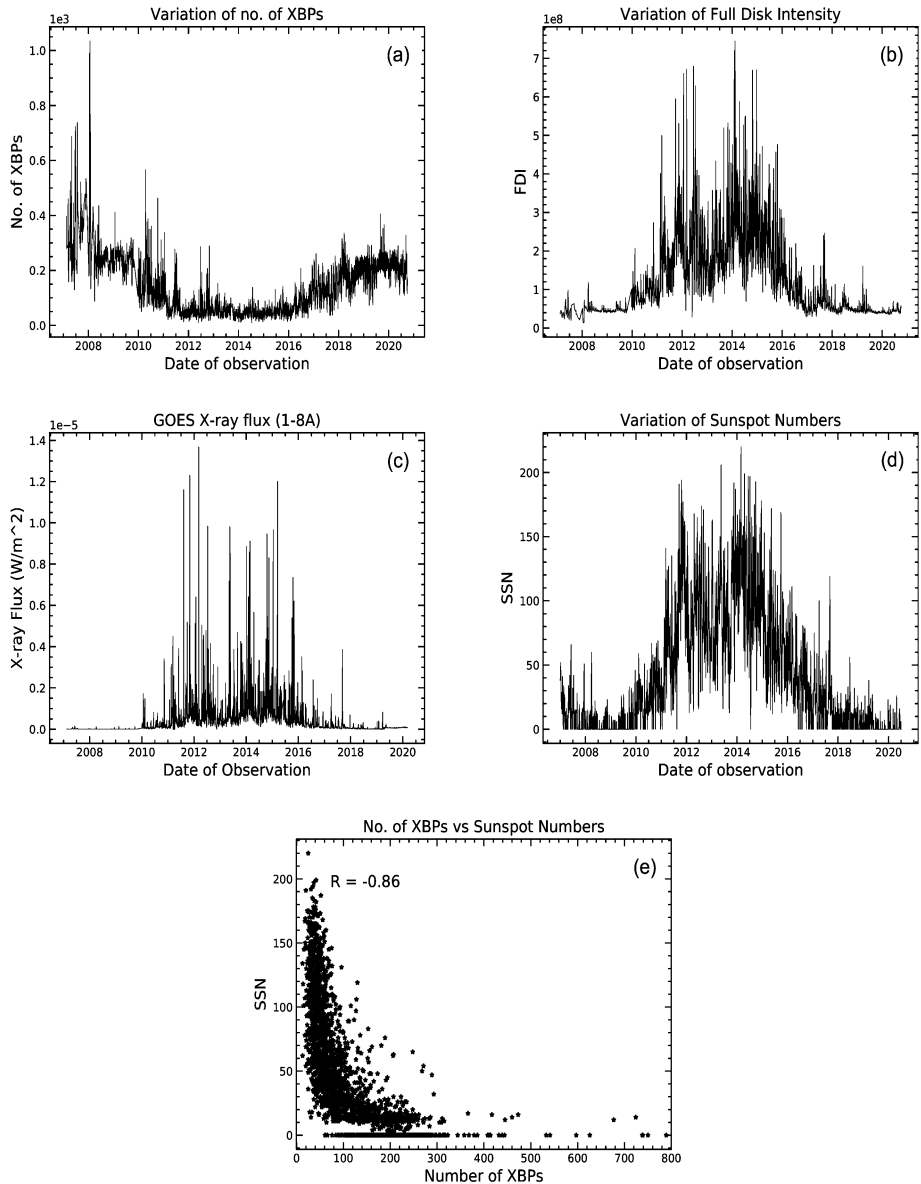


Figure 5 (a) Variation of the total number of XBPs using the AI_mesh filter, (b) FDI with the AI_mesh filter, (c) variation of GOES X-ray flux, (d) Sunspot number variation, and scatter plot: (e) number of XBPs with the AI_mesh versus SSN, for a period starting from February 14, 2007 to March 31, 2020.

number during solar maximum compared to that of the minimum phase. This suggests that the contribution of Ca II K bright points need to be taken into account in the reconstruction of integrated Ca II K line profile and to explain the chromospheric variability. So considering the large number of XBPs present at any time in the full-disk X-ray images and their number variation for the whole observed period, the contribution of XBPs can be considered in the

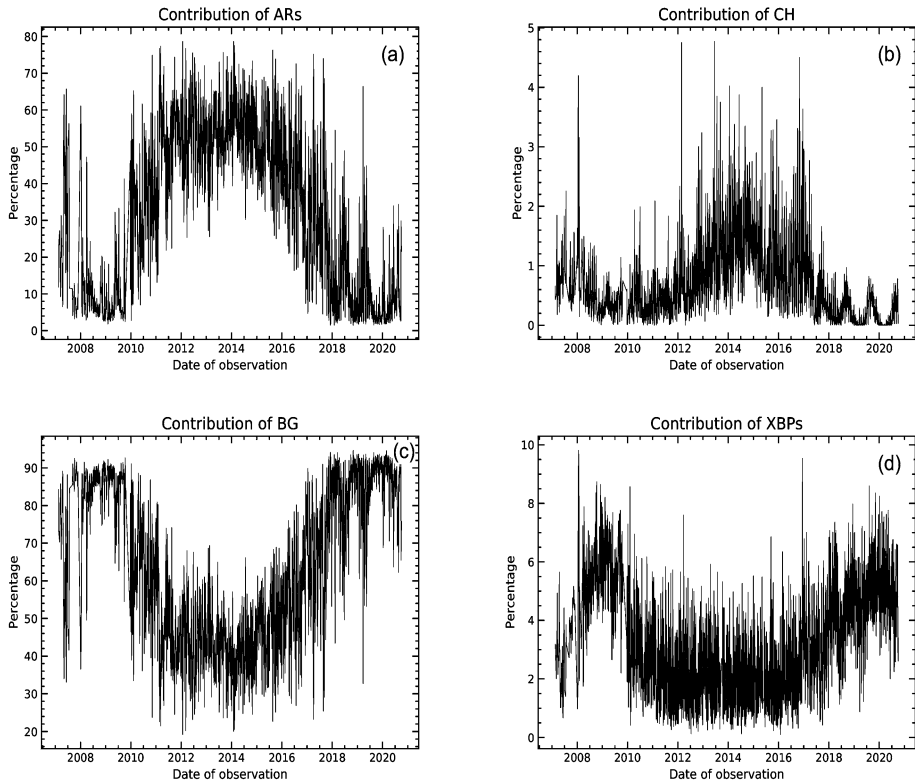


Figure 6 Variation of Contribution of ARs, CHs, BGs and XBPs to FDI with the Al_{mesh} filter: (a) ARs contribution variation, (b) CHs contribution variation, (c) BGs, and (d) XBPs contribution variations to FDI, for a period starting from February 14, 2007 to March 31, 2020.

reconstruction of solar X-ray irradiance variability. However, the physical reason for the existence of anti-correlation between the number variation of XBPs and solar activity cycle (SSN) needs to be understood by further detailed investigations. In order to confirm the existence of anti-correlation we are in the process of identifying and counting the XBPs over a quiet Sun region, preferably away from active regions, by different approaches for the entire period of observations to overcome the contamination and contribution of active regions (detailed results of such studies will be reported elsewhere).

3.3. Contribution of Coronal Features to Total Solar X-Ray Irradiance Variations

Since the full-disk intensity (FDI) and GOES solar X-ray flux values have been measured Sun as a star, they do not reveal directly the individual contribution of different features. In order to determine the contribution of the segmented X-ray features to FD intensity and X-ray irradiance variations we used an expression: contribution (%) = $(100 \times \text{intensity of the feature} / \text{FDI})$. Figure 6 represents the variation in the contribution of all the X-ray coronal features (ARs, CHs, BGs and XBPs) measured in Hinode/XRT with the Al_{mesh} filter to full-disk X-ray (FDI) irradiance variations. We noticed in Figure 6(a) and Figure 6(b) that the contribution of ARs and CHs changes with the phase of the solar cycle, whereas the BGs and XBPs contribution values, presented in Figure 6(c) and Figure 6(d), respectively, are

Table 2 Mean contribution (%) and corresponding standard deviation (Sigma) values determined in steps of 2 years for the periods: February 2007–2009, 2009–2011, 2011–2013, 2013–2015, 2015–2017, 2017–2019, and 2019–2020 March for all the features (ARs, BGs, CHs and XBPs) and FDI (DN/sec) and GOES X-ray flux (W/m^2).

Al_mesh Filter, Contribution plot (Figure 6)

	CHs	CHs	XBPs	XBPs	ARs	ARs
	Mean	Sigma	Mean	Sigma	Mean	Sigma
2007(Feb)-09	0.73	0.67	4.80	1.68	13.84	14.18
2009-11	0.37	0.49	4.11	1.06	25.50	15.61
2011-13	0.62	0.49	2.94	1.06	50.90	10.37
2013-15	1.34	0.67	1.94	0.94	53.77	08.13
2015-17	1.12	0.72	3.02	1.09	42.46	12.19
2017-19	0.37	0.39	3.80	1.35	17.15	14.38
2019-20(March)	0.17	0.20	5.43	1.07	08.68	07.85
Average	0.67	0.52	3.75	1.18	30.32	11.82

Al_mesh Filter, Contribution plot (Figure 6)

	BGs	BGs	FDI	FDI	GOES	GOES
	Mean	Sigma	Mean	Sigma	Mean	Sigma
2007(Feb)-09	80.63	13.04	$4.49E + 7$	$1.45E + 7$	$7.38E - 9$	$1.62E - 8$
2009-11	70.42	14.18	$7.54E + 7$	$2.91E + 7$	$8.70E - 8$	$1.94E - 7$
2011-13	46.55	9.78	$1.89E + 8$	$8.49E + 7$	$6.76E - 7$	$1.31E - 6$
2013-15	41.94	7.74	$2.34E + 8$	$10.24E + 7$	$9.28E - 7$	$1.05E - 6$
2015-17	53.40	11.54	$1.48E + 8$	$8.00E + 7$	$4.79E - 7$	$0.72E - 6$
2017-19	77.67	13.39	$0.57E + 8$	$2.06E + 7$	$0.56E - 7$	$1.35E - 7$
2019-20(March)	86.32	7.10	$0.45E + 8$	$0.87E + 7$	$0.65E - 7$	$0.48E - 7$
Average	65.28	10.97	$1.13E + 8$	$4.86E + 7$	$3.28E - 7$	$5.00E - 7$

inversely proportional to solar activity (large contribution during solar minimum and smaller during a solar maximum period). We also observed a similar behavior or pattern between the variations of the area (presented in Figure 3) and percentage of contributions (plotted in Figure 6) of all the coronal features, showing ARs and CHs vary in phase with the solar activity and whereas the BGs and XBPs are anti-correlated. To explain the physical reason for showing anti-correlation in the variation of the contribution of BGs and XBPs with the solar activity needs further investigations. In Table 2 we have presented the contribution values of all the features as a function of time. Figure 6 and Table 2 show that the background and active regions have a greater impact on the X-ray irradiance fluctuations and the average percentage of contributions to total solar X-ray flux from the BGs, ARs, XBPs, and CHs over the entire period of observations will be around 65%, 30%, 4% and 1%, respectively. We observe from Figure 6 and Table 2 that the BG regions are the main contributors to the total solar X-ray irradiance and covers a large area on the surface of the Sun. Similarly, ARs contribute about 30% and cover a smaller area on the Sun's surface, but they are brighter magnetic regions compared to other features. Hence the variations in both intensity and area of all the features need to be considered to explain the X-ray variability. That means the changes in both area and brightness will have more influence on the variation of total solar

X-ray irradiance. The XBPs will moderately contribute (around 4%) and CHs will have negligible contribution (about 1%) to the total solar X-ray irradiance variations.

The quiet-Sun component, combination of both BGs and XBPs of the corona, is estimated to vary due to the changing size of coronal holes and quiet-Sun regions. Considering the quiet-Sun variability we can notice that the quiet-Sun intensity also varies as a function of solar cycle and from this it is clear that there is no such thing that a 'solar constant or constant background emission in soft X-ray irradiance'. This confirms the earlier findings that the intensity of the quiet-Sun varies with the solar cycle as derived from Ca II K line observations near solar disk center in the chromospheric and temperature minimum regions (Kariyappa, 1999; Zhang et al., 2001). Hence, we conclude that the quiet-Sun is not quiet and constant, but it varies in phase with the solar activity and the changes are observed in the temperature minimum region, chromosphere, and in the corona. It is suggested that the contributions from the quiet-Sun are appreciable in the solar minimum and the soft X-ray (SXR) background flux appears to be dominated by post-flare emission from the dominant active regions and the evolution and confinement of heated plasma in flaring active regions will help to understand the variability of the full-disk integrated solar X-ray flux (Aschwanden, 1994).

We have estimated the mean contribution of the features to total X-ray irradiance in steps of every 2 years (2007–2009, 2009–2011, 2011–2013, 2013–2015, 2015–2017, 2017–2019, and 2019–2020) and the corresponding standard deviation values are also calculated for Figure 6. The reason for estimating for every 2 years is that during 2007 to 2020 (Solar Cycle 24) we find minimum, rase phase, maximum, declining phase and minimum in solar activity. The contribution of the features vary with the phase of the solar activity as discussed above. So we binned the time series into seven parts depending on the strength of the solar activity. In Table 2 we list the mean contribution for every 2 years and the values of standard deviation, and the average value of the contribution of all the features (ARs/CHs/BGs/XBPs/FDI/GOES) over the entire period of observation (2007 to 2020). It is clear from Figure 6 and Table 2 that BGs and ARs are the main contributors to total solar X-ray (SXR) flux. In addition, it suggests that the XBPs also contribute moderately to the GOES (1–8 Å) total solar X-ray flux variations, which cannot be neglected.

In this work, *for the first time*, we discussed in great detail the use of segmentation in resolved soft X-ray observations to measure X-ray irradiance fluctuations. The observations from Hinode/XRT helped us to segment the images into different individual X-ray features and to estimate and study their contribution to the total solar X-ray irradiance. Our algorithm is very sensitive to the different intensity levels, an effective one, capable to automatically identify and segment the coronal features from the images. We have shown that the X-ray Telescope onboard Hinode can be used to measure the solar X-ray (SXR) irradiance fluctuations. This allowed us to identify and extract different features including small-scale magnetic features like XBPs and to determine their contribution to the total solar X-ray irradiance. It is clear from Figure 6 and Table 2 that the background regions will have a large contribution to the solar X-ray irradiance, up to 65%, whereas the active regions contribute up to 30%. However, we observed that the contributions of XBPs and CHs are small (about average 4% and 1% respectively) compared to BGs and ARs. Although the XBPs are small in size, but they are intense magnetic regions and large in number at anytime over the whole solar disk. On the other hand, the XBPs will also play an important role in determining the intensity and temperature fluctuations and heating of the corona, since they are highly dynamic in nature (Kariyappa and Varghese, 2008; Kariyappa et al., 2011). In earlier studies (Kariyappa, Sivaraman, and Anadaram, 1994) it has been shown that the dynamical evolution of the bright points observed in Ca II H line will supply sufficient energy to maintain the chromospheric temperature and contribute to the heating of the quiet chromosphere

and to its variability. The XBPs have also been used as tracers in estimating the coronal rotational period (Kariyappa, 2008a; Kariyappa and DeLuca, 2012). In general, the different bright points, such as Ca II H and K BPs, UVBPs, He I dark-points, and XBPs, observed at different wavelengths will contribute to solar irradiance variability and heating of the solar atmosphere.

The segmented coronal features observed in X-ray wavelength can be used as proxies to isolate the underlying corresponding photospheric magnetic structures for further studies. In our future work we plan to extend our algorithm's capabilities to overlay the XRT full-disk segmented images/maps on to SOHO/MDI and SDO/HMI full-disk magnetograms and to segment the photospheric magnetic features corresponding to segmented coronal X-ray features. This would help us (i) to study the spatial correlation between coronal and photospheric magnetic features; (ii) to determine the total magnetic field of the segmented coronal features; (iii) to study the long-term variability of the integrated magnetic field of all the features; (iv) to quantify the role of magnetic field on the X-ray irradiance variability; (v) to understand the magnetic field fluctuations, and (vi) to construct the magnetic maps and total magnetic field of the corona. Such studies will have a wider scope for explaining the irradiance variability as all the X-ray features may be associated and related to underlying photospheric magnetic elements (since they are magnetic in origin). This research work is in progress. A similar investigations have been carried out and published recently by us (Zender et al., 2017) in the case of EUV and UV irradiance and magnetic field variabilities. In addition, for a future work, since the XRT instrument is producing the full-disk synoptic images with eight filters, we plan to use filter ratio method and the filters' response curves to generate the temperature maps of the full Sun using images with any two filters available, which are free from visible stray light contamination. Finally the temperature maps will be used to determine the temperature of the segmented features. This would help to understand the temperature fluctuations and long-term variations in temperature of all the segmented coronal features as a function of solar magnetic cycle. Recently we have studied the intensity variations and determined the temperature fluctuations in many XBPs observed with Hinode/XRT with two filters (Ti_poly and Al_mesh) by filter ratio method and using their response curves (Kariyappa and Varghese, 2008; Kariyappa et al., 2011).

Acknowledgements Hinode is a Japanese mission developed and launched by ISAS/JAXA, in collaboration with NAOJ as a domestic partner, NASA and STFC (UK) as international partners. The Hinode science team at ISAS/JAXA has conducted the Scientific operation of the Hinode mission. This team mainly consists of scientists from different institutes in the partner countries. JAXA and NAOJ (Japan), STFC (UK), NASA (USA), ESA, and NSC (Norway) have provided the support for the post-launch operation. The Hinode team had contributed all their efforts in the design, build, and operation of the mission. RK wishes to express his sincere thanks to all members of ISEE for the support provided under Joint International Research Program. A part of these results were presented by RK at the PSTEP-4 International Symposium held at ISEE/Nagoya University from January 28–30, 2020 and his visit to this symposium has been supported by MEXT/JSPS KAKENHI Grant Number JP15H05816. The authors are thankful to the referee for the valuable comments and suggestions that improved the manuscript considerably.

Disclosure of Potential Conflicts of Interest The authors declare that they have no conflicts of interest.

Publisher's Note Springer Nature remains neutral with regard to jurisdictional claims in published maps and institutional affiliations.

References

Acton, L.W., Weston, D.C., Bruner, M.E.: 1999, Deriving solar X ray irradiance from Yohkoh observations. *J. Geophys. Res.* **104**, 14827. DOI. ADS.

- Acton, L.W., Culhane, J.L., Gabriel, A.H., Bentley, R.D., Bowles, J.A., Firth, J.G., Finch, M.L., Gilbreth, C.W., Guttridge, P., Hayes, R.W., Joki, E.G., Jones, B.B., Kent, B.J., Leibacher, J.W., Nobles, R.A., Patrick, T.J., Phillips, K.J.H., Rapley, C.G., Sheather, P.H., Sherman, J.C., Stark, J.P., Springer, L.A., Turner, R.F., Wolfson, C.J.: 1980, The soft X-ray polychromator for the Solar Maximum Mission. *Solar Phys.* **65**, 53. DOI. ADS.
- Alipour, N., Safari, H.: 2015, Statistical properties of solar coronal bright points. *Astrophys. J.* **807**, 175. DOI. ADS.
- Arish, S., Javaherian, M., Safari, H., Amiri, A.: 2016, Extraction of active regions and coronal holes from EUV images using the unsupervised segmentation method in the Bayesian framework. *Solar Phys.* **291**, 1209. DOI. ADS.
- Aschwanden, M.J.: 1994, Irradiance observations of the 1–8 Å solar soft X-ray flux from goes. *Solar Phys.* **152**, 53. DOI. ADS.
- Bailey, S.M., Woods, T.N., Barth, C.A., Solomon, S.C., Canfield, L.R., Korde, R.: 2000, Measurements of the solar soft X-ray irradiance by the Student Nitric Oxide Explorer: first analysis and underflight calibrations. *J. Geophys. Res.* **105**, 27179. DOI. ADS.
- Bailey, S.M., Woods, T.N., Eparvier, F.G., Solomon, S.C.: 2006, Observations of the solar soft X-ray irradiance by the Student Nitric Oxide Explorer. *Adv. Space Res.* **37**, 209. DOI. ADS.
- de Wit, T.D.: 2006, Fast segmentation of solar extreme ultraviolet images. *Solar Phys.* **239**, 519. DOI. ADS.
- Dere, K.P., Horan, D.M., Kreplin, R.W.: 1974, The spectral dependence of solar soft X-ray flux values obtained by SOLRAD 9. *J. Atmos. Terr. Phys.* **36**, 989. DOI. ADS.
- Dorotovic, I., Coelho, A., Rybak, J., Mora, A., Ribeiro, R., Kusa, W., Pires, R.: 2018, Automatic detection and tracking of coronal bright points in SDO/AIA images. *Sun Geosph.* **13**, 129. DOI. ADS.
- Foukal, P., Lean, J.: 1988, Magnetic modulation of solar luminosity by photospheric activity. *Astrophys. J.* **328**, 347. DOI. ADS.
- Giono, G., Zender, J.J., Kariyappa, R., Damé, L.: 2021, Origin of the solar rotation harmonics seen in the EUV and UV irradiance. *Solar Phys.* submitted.
- Golub, L., DeLuca, E., Austin, G., Bookbinder, J., Caldwell, D., Cheimets, P., Cirtain, J., Cosmo, M., Reid, P., Sette, A., Weber, M., Sakao, T., Kano, R., Shibasaki, K., Hara, H., Tsuneta, S., Kumagai, K., Tamura, T., Shimojo, M., McCracken, J., Carpenter, J., Haight, H., Siler, R., Wright, E., Tucker, J., Rutledge, H., Barbera, M., Peres, G., Varisco, S.: 2007, The X-Ray Telescope (XRT) for the Hinode mission. *Solar Phys.* **243**, 63. DOI. ADS.
- Hall, L.A., Hinteregger, H.E.: 1970, Solar radiation in the extreme ultraviolet and its variation with solar rotation. *J. Geophys. Res.* **75**, 6959. DOI. ADS.
- Hara, H., Nakakubo-Morimoto, K.: 2003, Variation of the X-ray bright point number over the solar activity cycle. *Astrophys. J.* **589**, 1062. DOI. ADS.
- Hara, H., Nakakubo-Morimoto, K.: 2004, In: Sakurai, T., Sekii, T. (eds.) *Variation of the X-Ray Bright Point Number over the Solar Activity Cycle*, *Astronomical Society of the Pacific Conference Series* **325**, 307. ADS.
- Kariyappa, R.: 1999, Quiet-Sun variability with the solar cycle. In: Rimmele, T.R., Balasubramaniam, K.S., Radick, R.R. (eds.) *High Resolution Solar Physics: Theory, Observations, and Techniques*, *Astronomical Society of the Pacific Conference Series* **183**, 501. ADS.
- Kariyappa, R.: 2000, CaII K imaging to understand UV irradiance variability. *J. Astrophys. Astron.* **21**, 293. ADS.
- Kariyappa, R.: 2008a, Solar coronal rotation determined by X-ray bright points in Hinode/XRT and Yohkoh/SXT full-disc images. *Astron. Astrophys.* **488**, 297. DOI. ADS.
- Kariyappa, R.: 2008b, Spatially resolved images and solar irradiance variability. *J. Astrophys. Astron.* **29**, 159. DOI. ADS.
- Kariyappa, R., DeLuca, E.: 2012, Coronal rotation from XBPs observed with Hinode/XRT. In: Golub, L., De Moortel, I., Shimizu, T. (eds.) *Fifth Hinode Science Meeting*, *Astronomical Society of the Pacific Conference Series* **456**, 207. ADS.
- Kariyappa, R., Pap, J.M.: 1996, Contribution of chromospheric features to UV irradiance variability from spatially-resolved CA II K spectroheliograms. *Solar Phys.* **167**, 115. DOI. ADS.
- Kariyappa, R., Sivaraman, K.R.: 1994, Variability of the solar chromospheric network over the solar cycle. *Solar Phys.* **152**, 139. DOI. ADS.
- Kariyappa, R., Sivaraman, K.R., Anadaram, M.N.: 1994, Heating of the quiet solar chromosphere – part one. *Solar Phys.* **151**, 243. DOI. ADS.
- Kariyappa, R., Varghese, B.A.: 2008, Intensity oscillations and heating of the coronal X-ray bright points from Hinode/XRT. *Astron. Astrophys.* **485**, 289. DOI. ADS.
- Kariyappa, R., DeLuca, E.E., Saar, S.H., Golub, L., Damé, L., Pevtsov, A.A., Varghese, B.A.: 2011, Temperature variability in X-ray bright points observed with Hinode/XRT. *Astron. Astrophys.* **526**, A78. DOI. ADS.

- Kosugi, T., Matsuzaki, K., Sakao, T., Shimizu, T., Sone, Y., Tachikawa, S., Hashimoto, T., Minesugi, K., Ohnishi, A., Yamada, T., Tsuneta, S., Hara, H., Ichimoto, K., Suematsu, Y., Shimojo, M., Watanabe, T., Shimada, S., Davis, J.M., Hill, L.D., Owens, J.K., Title, A.M., Culhane, J.L., Harra, L.K., Doschek, G.A., Golub, L.: 2007, The Hinode (Solar-B) Mission: an overview. *Solar Phys.* **243**, 3. DOI. ADS.
- Kumara, S.T., Kariyappa, R., Dominique, M., Berghmans, D., Damé, L., Hochedez, J.F., Doddamani, V.H., Chitta, L.P.: 2012, Preliminary results on irradiance measurements from Lyra and Swap. *Adv. Astron.* **2012**, 623709. DOI. ADS.
- Kumara, S.T., Kariyappa, R., Zender, J.J., Giono, G., Delouille, V., Chitta, L.P., Damé, L., Hochedez, J.-F., Verbeeck, C., Mampaey, B., Doddamani, V.H.: 2014, Segmentation of coronal features to understand the solar EUV and UV irradiance variability. *Astron. Astrophys.* **561**, A9. DOI. ADS.
- Lean, J.: 1987, Solar ultraviolet irradiance variations – a review. *J. Geophys. Res.* **92**, 839. DOI. ADS.
- McIntosh, S.W.: 2007, On the mass and energy loading of extreme-UV bright points. *Astrophys. J.* **670**, 1401. DOI. ADS.
- McIntosh, S.W., Gurman, J.B.: 2005, Nine years of EUV bright points. *Solar Phys.* **228**, 285. DOI. ADS.
- Nakakubo, K., Hara, H.: 2000, Variation of X-ray bright point number over the solar activity cycle. *Adv. Space Res.* **25**, 1905. DOI. ADS.
- Ogawara, Y., Acton, L.W., Bentley, R.D., Bruner, M.E., Culhane, J.L., Hiei, E., Hirayama, T., Hudson, H.S., Kosugi, T., Lemen, J.R., Strong, K.T., Tsuneta, S., Uchida, Y., Watanabe, T., Yoshimori, M.: 1992, The status of Yohkoh in orbit: an introduction to the initial scientific results. *Publ. Astron. Soc. Japan* **44**, L41. ADS.
- Sattarov, I., Pevtsov, A.A., Hojaev, A.S., Sherdonov, C.T.: 2002, X-ray bright points and photospheric bipoles during cycles 22 and 23. *Astrophys. J.* **564**, 1042. DOI. ADS.
- Shahamatnia, E., Dorotović, I., Fonseca, J.M., Ribeiro, R.A.: 2016, An evolutionary computation based algorithm for calculating solar differential rotation by automatic tracking of coronal bright points. *J. Space Weather Space Clim.* **6**, A16. DOI. ADS.
- Sivaraman, K.R.: 1984, Ca II K bright points and the solar cycle. *Solar Phys.* **94**, 235. DOI. ADS.
- Takeda, A., Yoshimura, K., Saar, S.H.: 2016, The Hinode/XRT full-Sun image corrections and the improved synoptic composite image archive. *Solar Phys.* **291**, 317. DOI. ADS.
- Vaiana, G.S., Krieger, A.S., Timothy, A.F., Zombeck, M.: 1976, ATM observations, X-ray results. *Astrophys. Space Sci.* **39**, 75. DOI. ADS.
- van der Zwaard, R., Berghmann, M., Zender, J., Kariyappa, R., Giono, G., Damé, L.: 2021, Segmentation of coronal features to understand the solar EUV and UV irradiance variability III. Inclusion and Analysis of Bright points. *Solar Phys.* submitted.
- Veselovsky, I.S., Zhukov, A.N., Dmitriev, A.V., Tarsina, M.V., Clette, F., Cugnon, P., Hochedez, J.F.: 2001, Global asymmetry of the Sun observed in the Extreme Ultraviolet Radiation. *Solar Phys.* **201**, 27. ADS.
- Viereck, R.A., Machol, J.L.: 2017, *AGU Fall Meeting Abstracts #SH42A-06*. ADS.
- Worden, J.R., White, O.R., Woods, T.N.: 1998, Evolution of chromospheric structures derived from Ca II K spectroheliograms: implications for solar ultraviolet irradiance variability. *Astrophys. J.* **496**, 998. DOI. ADS.
- Zender, J.J., Kariyappa, R., Giono, G., Bergmann, M., Delouille, V., Damé, L., Hochedez, J.-F., Kumara, S.T.: 2017, Segmentation of photospheric magnetic elements corresponding to coronal features to understand the EUV and UV irradiance variability. *Astron. Astrophys.* **605**, A41. DOI. ADS.
- Zhang, Y.X., Fang, C., Ding, M.D., Livingston, W.C.: 2001, Quiet-Sun variability in a temperature minimum region. *Astrophys. J. Lett.* **547**, L179. DOI. ADS.

Solar Physics is a copyright of Springer, 2021. All Rights Reserved.